DOI https: //doi. org/10.1007/s11595-023-2721-5

Low-temperature Denitration Mechanism of NH_3-SCR over Fe/AC Catalyst

YANG Zhengyu[1,2], HUANG Bangfu[1,2*], ZHANG Guifang[1,2], DAI Meng[1,2], WEN Zhenjing[1,2], LI Wanjun[1,2]

(1. Faculty of Metallurgical and Energy Engineering, Kunming University of Science and Technology, Kunming 650093, China; 2. Clean Metallurgy Key Laboratory of Complex Iron Resources, University of Yunnan Province, Kunming 650093, China)

Abstract: To study the modification mechanism of activated carbon (AC) by Fe and the low-temperature NH_3-selective catalytic reduction (SCR) denitration mechanism of Fe/AC catalysts, Fe/AC catalysts were prepared using coconut shell AC activated by nitric acid as the support and iron oxide as the active component. The crystal structure, surface morphology, pore structure, functional groups and valence states of the active components of Fe/AC catalysts were characterised by X-ray diffraction, scanning electron microscopy, nitrogen adsorption and desorption, Fourier transform infrared spectroscopy and X-ray photoelectron spectroscopy, respectively. The effect of Fe loading and calcination temperature on the low-temperature denitration of NH_3-SCR over Fe/AC catalysts was studied using NH_3 as the reducing gas at low temperature (150 ℃). The results show that the iron oxide on the Fe/AC catalyst is spherical and uniformly dispersed on the surface of AC, thereby improving the crystallisation performance and increasing the number of active sites and specific surface area on AC in contact with the reaction gas. Hence, a rapid NH_3-SCR reaction was realised. When the roasting temperature remains constant, the iron oxide crystals formed by increasing the amount of loading can enter the AC pore structure and accumulate to form more micropores. When the roasting temperature is raised from 400 to 500 ℃, the iron oxide is mainly transformed from α-Fe_2O_3 to γ-Fe_2O_3, which improves the iron oxide dispersion and increases its denitration active site, allowing gas adsorption. When the Fe loading amount is 10%, and the roasting temperature is 500 ℃, the NO removal rate of the Fe/AC catalyst can reach 95%. According to the study, the low-temperature NH_3-SCR mechanism of Fe/AC catalyst is proposed, in which the redox reaction between Fe^{2+} and Fe^{3+} will facilitate the formation of reactive oxygen vacancies, which increases the amount of oxygen adsorption on the surface, especially the increase in surface acid sites, and promotes and adsorbs more reaction gases (NH_3, O_2, NO). The transformation from the standard SCR reaction to the fast SCR reaction is accelerated.

Key words: nitric acid activation method; coconut shell activated carbon; Fe/AC catalyst; NH_3-SCR; low-temperature denitrification mechanism

1 Introduction

The iron and steel industry is an important establishment of a nation's economy. Sintering is one of the most polluting processes in the iron and steel production processes, with high energy consumption, high flue gas emissions and serious pollution. It contains NO_x pollutants that cause serious harm to human life, health and the ecological environment[1-3]. Currently, the main technologies for the denitrification of sintering flue gas include physical adsorption, forced oxidation, catalytic oxidation, selective catalytic reduction (SCR) and other methods, with SCR is commonly used in industry because of its high denitrification rate[4,5], and the core of the its catalyst. In industries, V_2O_5-WO_3/TiO_2 catalyst is widely used. It has been commonly used in thermal power plants and coal-fired boilers, but its operating temperature window is too high, generally between 300 and 400 ℃. There have been numerous domestic and foreign reports on the research of different types of low-temperature NO_x removal catalysts[6-8]. Currently, one of the main carriers of low-temperature NO_x removal catalysts is AC. Among them, coconut shell AC has a large specific surface area, rich pore structure, good adsorption performance, high mechanical strength and stable

© Wuhan University of Technology and Springer-Verlag GmbH Germany, Part of Springer Nature 2023

(Received: Nov. 29, 2022; Accepted: Feb. 18, 2023)

YANG Zhengyu(杨征宇): E-mail: 983974123@qq.com

*Corresponding author: HUANG Bangfu(黄帮福): Assoc. Prof.; Ph D; E-mail: 595762307@qq.com

Funded by the General Project of Science and Technology Plan of Yunnan Science and Technology Department (Nos.202001AT070029, 2019FB077), Open Fund of Key Laboratory for Ferrous Metallurgy and Resources Utilization of Ministry of Education (No. FMRUlab-20-4)

chemical properties, allowing for treating multiple pollutants in the sintering flue gas to be coordinated[9,10]. However, when coconut shell AC is used as an adsorbent, its denitration performance is limited, and it cannot achieve ultra-low emission directly. Therefore, developing high-efficiency SCR catalysts with low-temperature activity is critical for treating sintering flue gas.

Several studies have shown that coconut shell AC should be activated by various acids[11,12] to destroy its pore structure, change the mesopores into a micropore, and change the pore volume and specific surface to enhance its adsorption performance. The metal-doping modification improves the catalyst structure, component activity and denitration performance of coconut shell AC, achieving an ultra-low emission. Currently, catalysts containing transition elements[13-15] (V, Fe, Mn, Cu, *etc*) and rare earth elements[16-18] (Ce, Ho, *etc*) as active metal components exhibit good denitration activity at temperatures below 200 ℃. Among them, Fe_2O_3 is a good catalyst active substance in the NO reaction and has the best dispersion on the AC surface, and the active site of NO molecular activation is related to Fe_2O_3 species[19-21]. Xie *et al*[22] found that NH_3 molecules chemically absorb with Fe_xO_y/AC surface-active Fe atoms to form coordination NH_3, which is conducive to NH_3 adsorption and thus accelerates the NH_3-SCR denitration reaction. Liang *et al*[23] used nano-sized γ-Fe_2O_3 as a catalyst to conduct experiments at low-temperature experiments, and the results showed that nano-sized γ-Fe_2O_3 catalyst has good NO_x removal activity, with a NO_x removal efficiency of 97% under aerobic conditions. These experimental studies demonstrate that Fe/AC catalyst exhibits excellent NO_x removal efficiency and is suitable for development as a removal NO_x removal catalyst. Currently, there are few reports on the effect of different iron crystal oxides on the catalyst activity. Among them, γ-Fe_2O_3 is a commonly used magnetic material that has a wider active temperature window, better SCR activity, higher nitrogen selectivity and wider active temperature window than α-Fe_2O_3[24,25]. However, the mechanism of AC modification by Fe_2O_3 and the influence mechanism of α-Fe_2O_3 and γ-Fe_2O_3 on denitration in the low-temperature denitration process have not been fully revealed.

To clarify the modification mechanism of AC by Fe after nitric acid activation and the low-temperature NH_3-SCR denitration mechanism of Fe/AC catalyst, the Fe/AC catalysts were prepared with coconut shell AC after activation of nitric acid using a constant volume ultrasonic impregnation method. The Fe/AC catalysts were characterised using SEM, BET, FITR, XRD and XPS. The modification mechanism of Fe/AC catalysts with different roasting temperatures and Fe loading were investigated, including changes in pore structure, specific surface area, active substance and acidic oxygen-containing functional groups. The influence mechanism of α-Fe_2O_3 and γ-Fe_2O_3 on denitration over Fe/AC catalysts in the process of low-temperature denitration process was investigated.

2 Experimental

2.1 Material

Iron nitrate ($Fe(NO_3)_3 \cdot 9H_2O$), analytically pure, was produced by Tianjin Komio Chemical Reagent Co., Ltd. Coconut shell AC (particle size of 20-40 mesh) was from Henan Gongyi Lantian Water Purification Technology Co., Ltd. The water used in the experiment was deionised.

2.2 Preparation of Fe/AC

The coconut shell AC was sieved to 20-40 mesh and deionised by water 6-7 times to remove surface ash. Then, the water bath was heated at 60 ℃ for 2 h at a constant temperature. After filtration, it was placed in a blast-drying oven at 110 ℃ for 12 h (marked as AC). The coconut shell AC (marked as HNO_3/AC) was activated by nitric acid at 80 ℃ for 2 h. Then, four portions of HNO_3/AC, each with a mass of 20.00 g, were soaked in 5% and 10% $Fe(NO_3)_3$ solution at room temperature. The HNO_3/AC was immersed in water bath at 60 ℃ for 2 h before drying in a clean air-blast-drying oven at 110 ℃ for 12 h. After drying, the Fe/AC catalysts were prepared by roasting at different temperatures in an N_2 atmosphere at 400 and 500 ℃ for 4 h until the $Fe(NO_3)_3$ was completely decomposed. The Fe/AC catalysts were recorded as Fe/AC-1 (5%, 400 ℃), Fe/AC-2 (10%, 400 ℃), Fe/AC-3 (5%, 500 ℃) and Fe/AC-4 (10%, 500 ℃).

2.3 Catalyst characterisation

The load metal oxide was estimated using a rotating target XRD (TTR18 kW Cu target) to analyse the crystal phase pattern of Fe/AC, and the surface microstructure change of Fe/AC was observed using SEM (Tescan VEGAS SBH), nitrogen adsorption and a desorption tester, and the N_2 adsorption isotherm was used (BET, QDS-evo). At 77 K, the specific surface area, pore volume and average pore diameter of Fe/AC were measured, and the micropore volume was

calculated using the Dubinin–Radushkevich method. Each sample was degassed under vacuum at 200 ℃ for 4 h before the N_2 adsorption. The surface functional group changes of the Fe/AC catalysts were measured using FTIR (Nicolet iS 10) in the range of 4 000-400 cm^{-1}, and the surface atomic state of the catalysts was analysed using XPS (PHI5000 Versaprobe-II) at 50 W using AlKα X-ray (hv = 1 486.6 eV) radiation. A C1s-binding energy (BE) value of 284.8 eV was used to calibrate the BE.

2.4 Denitration activity test

The denitration activity test of the Fe/AC catalysts was conducted in a fixed-bed reactor. Fig.1 shows the catalyst denitration reaction device, which consists of a gas metering and mixing system, a reaction system and a tail gas detection system. At the same temperature, the denitration activity of Fe/AC with different loads was tested. The thermocouple in the tubular reactor was used to measure the reaction temperature; based on the measured temperature, the furnace temperature was adjusted, reaction temperature was determined and the simulated flue gas was passed into the reactor. The simulated flue gas (NO) flow rate was 40 mL·min^{-1}, the NH_3 flow rate was 40 mL·min^{-1}, and the O_2 flow rate was 120 mL·min^{-1} (10%). The balance gas was N_2, the total gas flow rate was 1 200 mL, the flow rate was 40 mL·$min^{-1,}$ and the GHSV was 30 000 h^{-1}. The final exhaust gas was detected using a Testo-340 flue gas analyser (Germany Testo Instruments) for 60 min.

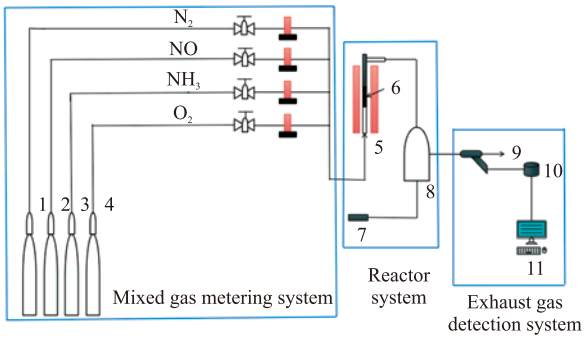

Fig.1 Catalyst denitration reaction device
1. N_2; 2. NO; 3. NH_3; 4. O_2; 5. Vertical fixed bed; 6. Catalysts; 7. Tail gas treatment unit; 8. Gas buffer bottle; 9. Detection gun; 10. Flue gas analyser; 11. Computer for analysis

The conversion rate of NO_x was calculated using the following formula:

$$\eta = \frac{C_{in(NO)} - C_{out(NO+NO_2)}}{C_{in(NO)}}$$

where $C_{in(NO)}$ is the NO concentration at the reactor inlet, ppm; $C_{out(NO+NO_2)}$ is the NO + NO_2 concentration at the reactor outlet, ppm; and η is the denitration rate, %.

3 Results and discussion

3.1 XRD analysis

Fig.2 shows the XRD patterns of AC after hydrothermal treatment and HNO_3/AC after nitric acid activation. The figure shows that after carbon or nitric activation, AC was mainly composed of graphite crystallites. Therefore, graphite peaks are usually found in the XRD pattern. The two types of AC are 23.813° and 43.467° (100 crystal planes) in 2θ. Each position has a wide dispersion characteristic peak, indicating that the coconut shell AC is mainly composed of amorphous carbon. The peak at 23.813° is the diffraction peak of loosely stacked graphene layers, and the peak at 43.467° is graphite crystals. The diffraction peak, the sharp peak at 26.468° in the figure, is the diffraction peak of the graphite (002) crystal plane [26], indicating that the diffraction peak of the graphene layer and graphite crystal becomes sharp and enhanced after nitric acid activation treatment. As shown in Fig. 3, according to the standard card of α-Fe_2O_3 (JCPDS Card No.33-664), the peaks at 2θ of 24.123°, 35.569°, 49.378°, 53.988°, 57.409° and 62.381° correspond to the diffraction peaks of α-Fe_2O_3. From the standard card of γ-Fe_2O_3 (JCPDS Card No.39-1346) in the figure, the diffraction peak of γ-Fe_2O_3 is at 30.109°, 33.088°, 35.735°, 43.216°, 43.412°, 57.732° and

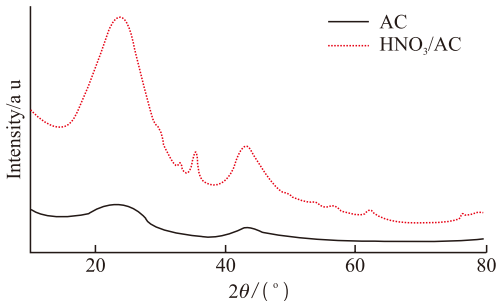

Fig.2 XRD pattern of AC and HNO_3/AC

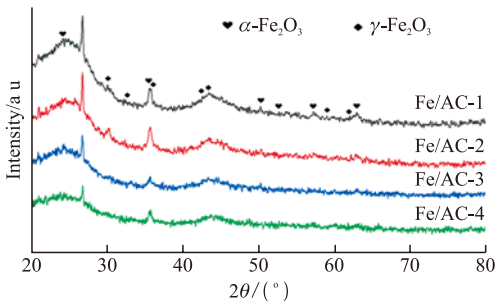

Fig.3 XRD pattern of Fe/AC catalysts

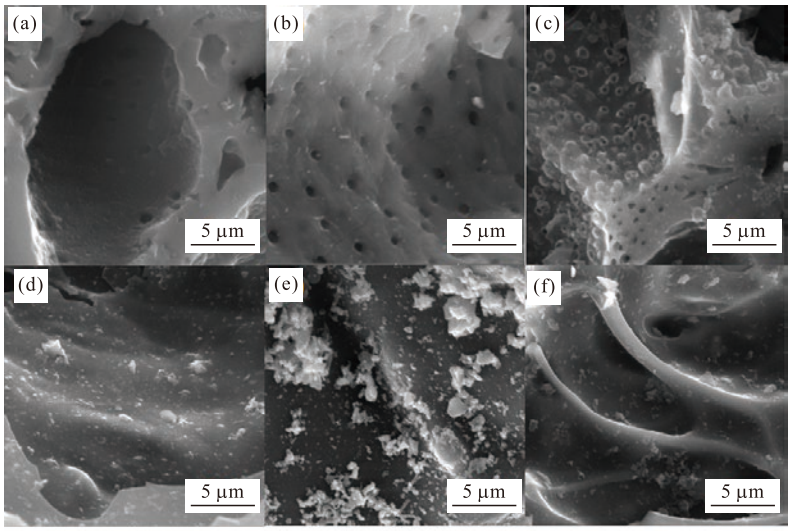

Fig.4 SEM micrographs of different catalysts: (a) AC; (b) HNO_3/AC; (c) Fe/AC-1; (d) Fe/AC-2; (e) Fe/AC-3; (f) Fe/AC-4

62.991°. The XRD patterns of Fe/AC-1, 2 show that the peaks at 2θ of 24.123°, 35.569°, 49.378°, 57.409° and 62.381° correspond to the diffraction peak of α-Fe_2O_3, and the diffraction peak of γ-Fe_2O_3 at 30.255°, as shown in Fig.3. The results show that there is a significant amount of α-Fe_2O_3 in the iron oxides formed by roasting iron nitrate at 400 ℃, as well as a part of γ-Fe_2O_3. The XRD pattern of Fe/AC-3, 4 shows that the diffraction peak of γ-Fe_2O_3 corresponds to the peak at 2θ of 30.109°, 35.735°, 43.216°, 43.412°, 57.732° and 62.381°, and a small peak of γ-Fe_2O_3 at 33.236°, and the diffraction peak at 35.735° has sharp symmetry, indicating that the iron oxides produced by roasting iron nitrate at 500 ℃ are mainly γ-Fe_2O_3 crystals, and only part of α-Fe_2O_3 exists. It was concluded that with the increase of roasting temperature from 400 to 500 ℃, γ-Fe_2O_3 crystal cells gradually grow up, the degree of crystallisation increases, and the lattice diffraction peak increases, while the characteristic peak of α-Fe_2O_3 weakens, and the α-type crystal cell structure changes to γ-type[27]. The XRD diagram of Fe/AC-4 shows that the peaks at various angles are not sharp, indicating that the dispersion of γ-Fe_2O_3 on AC load is more uniform, and the crystallisation performance is better.

3.2 SEM analysis

SEM characterisation was conducted to further study the changes in the surface morphology of the material before and after AC loading Fe, and the results are shown in Fig.4. Due to different loading and calcination temperatures, the iron oxides present different granular spheres on the surface and pores of coconut shell AC under the same immersion time condition. A scanning electron micrograph with a 10 000 times magnification is shown in Fig.4. According to Fig.4(a) and (b) of the AC of coconut shell before Fe loading, the AC of coconut shell without treatment has developed a pore structure, smooth surface and clear pore structure. After activation by nitric acid, the AC of the coconut shell showed an obvious porous structure in the same region, with mainly microporous and smooth pore walls, indicating that the coconut shell AC had improved physical and chemical properties, as well as enhanced adsorption performance. The surface morphology of the catalyst changed after impregnation with $Fe(NO_3)_3$. The pore structure of the coconut shell AC carrier was still retained after loading Fe. Few particles were dispersed in the pores of AC, as shown in Figs.4(c) and 4(d). As the loading capacity increased, iron oxide was uniformly dispersed on the surface of the AC channel (Fig.4(e) and 4(f)). The catalyst particles were spherical with uniform size, thereby drastically increasing the number of active sites and specific surface area in contact with the reaction gas. Most iron oxides (the main body is α-Fe_2O_3) generated by roasting iron nitrate at high temperatures are attached to the surface of the coconut shell AC with a certain thickness plate, as shown in Fig.4(e). The pores of coconut shell AC have irregular granular crystals and few blocks embedded in the pores, indicating poor dispersion of the iron oxides. The pore structure of AC is visible, iron oxide (the main body is γ-Fe_2O_3) is spread on the surface and pore structure of AC, and some small pieces are embedded in the pores of the AC, and the connectivity between the pores is good, relatively independent without adhesion, and no large plate is found, as shown in (f). Therefore, comparing Fe/AC-3 with Fe/AC-4 showed that when the roasting temperature was 400 ℃, the

main iron oxide was α-Fe_2O_3, and the pore of AC was blocked, affecting the denitrification performance of the modified AC. When the roasting temperature is 500 ℃, the iron oxide crystals can enter the pore structure of AC and accumulate to form more micropores. Iron nitrate mainly formed γ-Fe_2O_3. The increase in roasting temperature improves the dispersion of iron oxides and makes the load γ-Fe_2O_3 distribution more uniform. Simultaneously, it also accords with the XRD analysis results.

3.3 BET analysis

The specific surface area of a catalyst affects its SCR denitration activity to some extent, and a larger specific surface area can provide more active sites for the reaction. Hence, the increased contact area between the reaction gas and the catalyst surface accelerates the denitration reaction. Therefore, the BET was used to characterise and analyse the Fe/AC catalysts. The specific surface area, average pore volume and pore size of Fe/AC catalysts are shown in Table 1. The nitrogen isothermal adsorption-desorption curve and the pore size distribution of Fe/AC catalysts are shown in Fig.5 and Fig.6. According to the IUPAC classification, it is type IV isotherms with H1-type hysteresis loops[28,29], indicating that the structures have highly ordered micropore channels, which is similar to the SEM results. In summary, the specific surface area of AC decreased after nitric acid activation treatment. After nitric acid activation, the average pore size of AC decreases while the average pore volume increases. This is because nitric acid activation removes the ash on the original pore while generating new pores. The carbon skeleton of AC will shrink during the Fe/AC roasting process at high temperatures in a nitrogen atmosphere, reducing the size of the original pores. In the process of impregnation of AC, Fe^{3+} can enter the pore of AC. In the process of roasting $Fe(NO_3)_3$ at high temperatures, the crystal position will become the heat aggregation point, resulting in the ablation of part of AC. The interior pore structure of AC can be developed. In the Fe/AC prepared by roasting with equal volume impregnation of $Fe(NO_3)_3$, Fe/AC-4 is the best, and the micropore volume, micropore specific surface area, total pore volume and total specific surface area are the highest among the four types of Fe/AC, indicating that as loading capacity increases, some small pores are blocked, which increases the average pore size. However, this will not affect the increase in the specific surface area or denitration reaction. As the number of active components increases, new channels will be generated based on the original AC channels. Iron oxide is mainly transformed from α-Fe_2O_3, blocking the pores of AC to γ-Fe_2O_3 with a more uniform dispersion, which is also verified by the SEM and XRD analysis results.

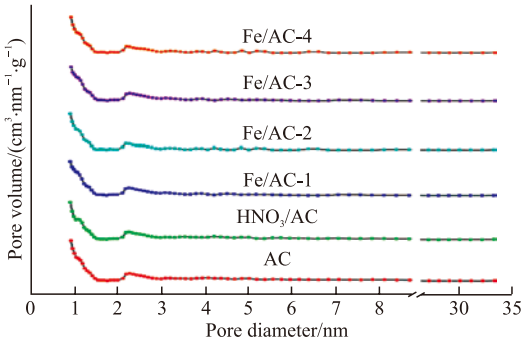

Fig.5 Pore diameter distribution

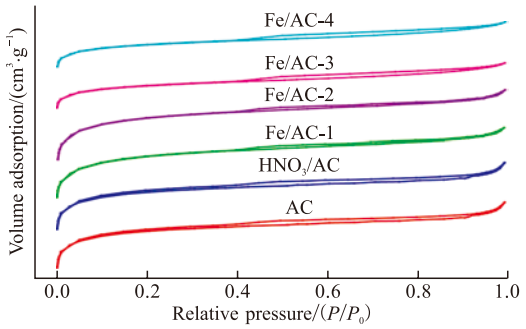

Fig.6 N_2 adsorption-desorption

Table 1 Specific surface area and pore structure of Fe/AC

Fe/AC	Specific surface /(m^2/g)	Pore volume /(cm^3/g)	Pore size /nm
AC	768.690	0.383	2.201
HNO_3/AC	654.086	0.393	2.206
Fe/AC-1	782.483	0.401	2.211
Fe/AC-2	810.067	0.413	2.218
Fe/AC-3	791.931	0.408	2.215
Fe/AC-4	815.087	0.421	2.223

3.4 FTIR analysis

The surface chemical properties of coconut shell AC are mainly determined by the type and quantity of surface functional groups, and most of the functional groups on the surface of AC are oxygen-containing functional groups, such as carboxyl, phenolic hydroxyl, carbonyl, ester and ether groups [30]. After HNO_3 activation treatment, AC is somewhat ablated, releasing CO and CO_2[31]. The basic pore structure shows partial defects, and O and H are adsorbed on the pores to form various oxygen-containing functional groups[32]. The FTIR spectra after nitric acid activation and metal oxide loading are shown in Fig.7 and Fig.8, respectively.

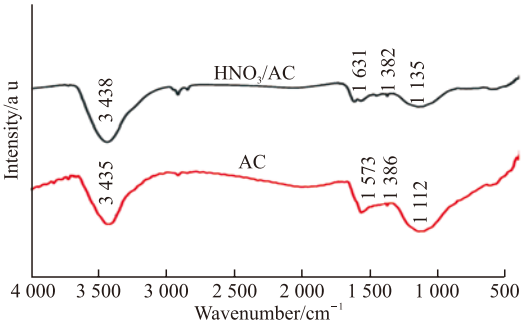

Fig.7 FTIR spectrogram of AC and HNO_3/AC

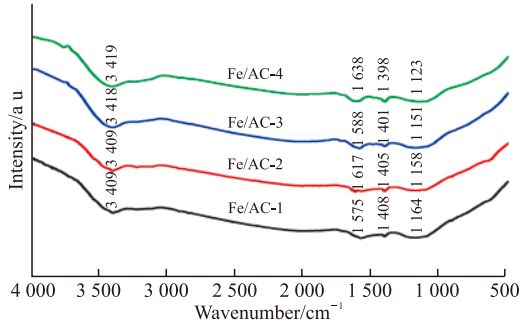

Fig.8 FTIR spectrogram of Fe/AC

According to a previous study[33-35], the infrared band 3 600-3 200 cm^{-1} is attributed to the stretching vibration of –OH; the infrared band 1 740-1 480 cm^{-1} is attributed to the stretching vibration of C=O or C=C. The 1 300-1 000 cm^{-1} band is attributed to C–O–C or C–O stretching vibrations. Fig.7 shows that after activation with nitric acid, the AC spectrum shows clear peaks at 3 438 cm^{-1} (–OH stretching vibration), 1 573 cm^{-1} (–C=O stretching vibration) and 1 135 cm^{-1} (–CO stretching vibration). After nitric acid activation, the state was enhanced, and two new absorption peaks appeared at 1 631 cm^{-1}(–C=O stretching vibration) and 1 450 cm^{-1}(–CH). More acidic oxygen-containing and nitrogen-containing functional groups, such as carboxyl groups, lactone groups, hydroxyl groups and nitro groups, which are easy to react with NO, are formed on the AC surface after nitric acid activation[36,37]. The basic types of Fe/AC functional groups are the same under different loading and calcination temperatures, as shown in Fig.8. However, as the calcination temperature increased, the -OH stretching vibration absorption peak in the -COOH of 3 419 cm^{-1} and chemically adsorbed water was enhanced, and the asymmetric vibration absorption peak of 1 638 cm^{-1} lactone group becomes more obvious. The results showed that as the roasting temperature increased, the adsorption sites of oxygen-containing functional groups on the AC surface, such as carboxyl and lactone groups, increased continuously, and the increase in oxygen-containing functional groups would provide more active sites for the denitration reaction, as well as, more highly adsorbed oxygen (O_β) for the first stage of the denitration reaction[38], thus promoting the denitration reaction of NH_3-SCR.

3.5 XPS analysis

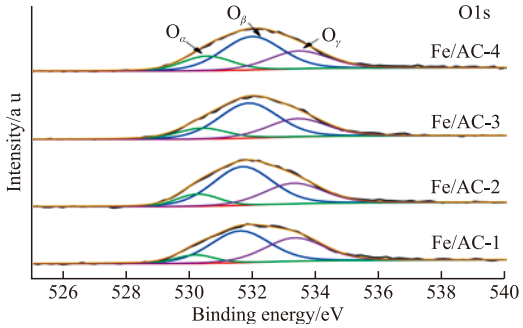

Fig.9 XPS survey spectrum of O1s

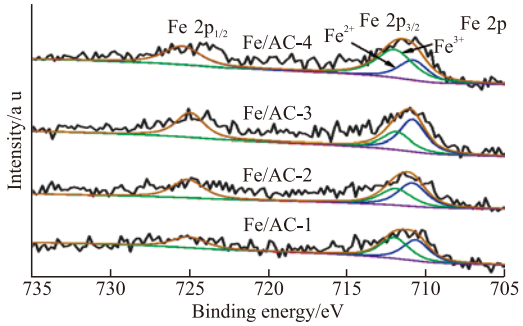

Fig.10 XPS survey spectrum of Fe2p

This experiment used XPS characterisation on the Fe/AC catalysts activated by nitric acid before denitration to study the valence state and proportion of active elements on the surface of the catalyst. The figures show the energy spectra of O1s and Fe2p orbitals. The energy spectra of the Fe2p orbitals of different samples are described in Fig.10. The Fe2p of each catalyst showed two obvious strong peaks, corresponding to Fe2p3/2 (BE about 711 eV) and Fe2p1/2 (BE about 725 eV), respectively. The binding energies of Fe2p3/2 were 710.7 and 712.5 eV, which correspond to Fe^{2+} and Fe^{3+}, respectively, indicating that Fe coexisted with Fe^{2+} and Fe^{3+} in the four catalysts. The O1s spectra of different samples are shown in Fig.9. Because of the unique surface structure of AC, the surface oxygen species can be classified as lattice oxygen (O_α), surface-adsorbed oxygen (O_β) and chemical oxygen (O_γ)[39]. Fitting the peaks of O1s yielded three peaks with binding energies of approximately 530.1, 532.8 and 531.3 eV, corresponding to O_α, O_γ and O_β, respectively. The increase in the Fe/AC-4 catalyst (O_β) ratio, *i e*, ((O_β) / (O_α) + (O_β) + (O_γ)), was pronounced. However, as

shown in the FTIR diagram, nitric acid activation produced more hydroxyl and carbonyl groups in addition to other oxygen-containing functional groups. However, as the roasting temperature increased, a redox reaction occurred between Fe^{2+} and Fe^{3+}, forming more active oxygen vacancies, thereby increasing O_β, *i e*, the amount of oxygen adsorbed on the surface. In summary, as the roasting temperature increased, the content of γ-Fe_2O_3 significantly increased, resulting in a significant increase in the Fe^{3+} content (Fe^{3+}/Fe^{2+} + Fe^{3+}), allowing the catalyst surface to have more surface adsorption oxygen (O_β), which has a higher flow rate. Simultaneously, the results of XRD were verified.

4 Influence of Fe loading and roasting temperature on the denitration activity of Fe/AC

In the experiment, the denitration activity of the prepared catalyst was measured to investigate the mechanism of the effect of Fe loading and roasting temperature on the denitration mechanism of NH_3-SCR. In the presence of GHSV of 30 000 h^{-1} and 10% O_2, low-temperature NH_3-SCR denitrification activity of Fe/AC catalysts loaded with AC at different loadings and calcination temperatures at 150 ℃ was studied. Fig.7 showed that the denitration effect of HNO_3/AC after nitric acid activation is higher than that of AC after hydrothermal treatment. This may be due to the formation of oxygen-containing functional groups due to the activation of nitric acid, which promotes the adsorption and oxidation of NO [40], allowing metal oxides to disperse in AC. When the roasting temperature is 400 ℃, the NO conversion rate is relatively low, which may be because the metal oxides on the AC surface are mainly α-Fe_2O_3. As the proportion of α-Fe_2O_3 increases, the pores of the AC will be blocked, affecting the denitration activity of the Fe/AC catalyst. When the roasting temperature is 500 ℃, the denitrification efficiency is relatively stable, reaching >90%. It is possible that the AC surface metal oxides, mainly γ-Fe_2O_3, will significantly increase, resulting in Fe/AC having good thermal stability and an increase in surface adsorption oxygen, especially with the increase of surface acid sites and the adsorption of more reactive gases[41,42]. In conclusion, when the roasting temperature is 500 ℃, the denitration efficiency of the Fe/AC-4 catalyst is the highest, which may be attributed to an increase of surface-adsorbed oxygen, which may help to improve the catalytic activity of γ-Fe_2O_3 in NH_3-SCR reaction [43].

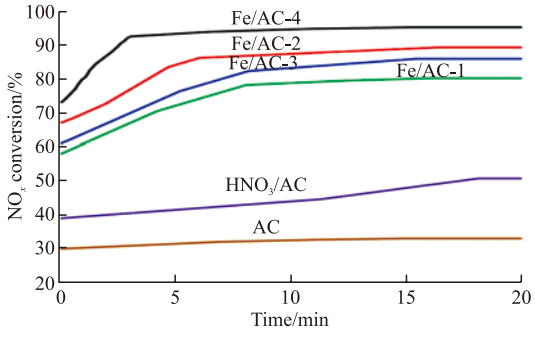

Fig.11 NO_x conversion for different Fe/AC catalysts

5 Mechanism research

5.1 Modification mechanism of AC by Fe

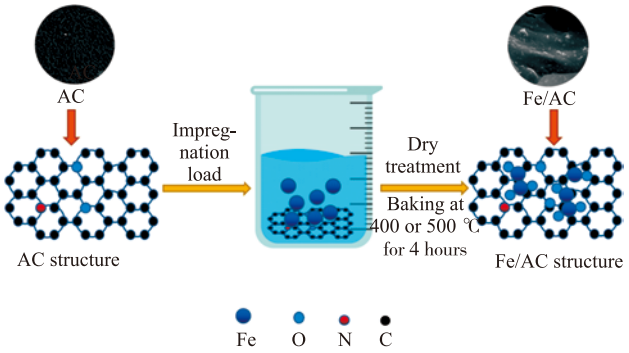

Fig.12 Schematic diagram of the preparation of Fe/AC catalyst

As a carbon-based carrier of porous catalysts, AC has numerous tiny channels, and its structure with abundant graphite microcrystals can provide a surface for gas–solid reactions. AC was used as the basis for Fe/AC catalysts. During the impregnation process, the AC carrier is immersed in $Fe(NO_3)_3$ mixed solutions with different mass fractions required by an ultrasonic water bath at a temperature of 60 ℃ to make the metal ions move vigorously into the interior of the AC carrier void and attach to the AC surface during the drying process. In the process of N_2 protective roasting, $Fe(NO_3)_3$ decomposes into different crystalline iron oxides at 400 and 500 ℃. As shown in the XRD figure, as the increase of roasting temperature increased, the number of γ-Fe_2O_3 crystal cells increased, as did the degree of crystallisation, and the lattice diffraction peak increased, while the characteristic peak of α-Fe_2O_3 weakened, and α-Fe_2O_3 to γ-Fe_2O_3 transformation. As shown in the XPS diagram, the redox reaction between Fe^{2+} and Fe^{3+} formed more active oxygen vacancies, which increased the amount of oxygen adsorption

(O_β) on the surface. As shown in the FTIR diagram, the number of adsorption sites, such as carboxyl and lactone groups containing oxygen-functional groups on the AC surface, increased continuously as the roasting temperature increased. The increase in oxygen-functional groups will provide more active sites for denitration and provide more highly adsorbed oxygen (O_β) for the first stage of denitrification. The Fe/AC catalysts' preparation schematic diagram is shown in Fig.12.

5.2 Mechanism of low-temperature NH_3-SCR denitration on Fe/AC catalysts

Based on these characterisation observations, the NH_3-SCR low- temperature denitration reaction on the Fe/AC catalyst surface is a representative heterogeneous reaction. The NH_3-SCR denitrification mechanism is proposed based on the characterisation results, as shown in Fig.13, and can be divided into three steps:

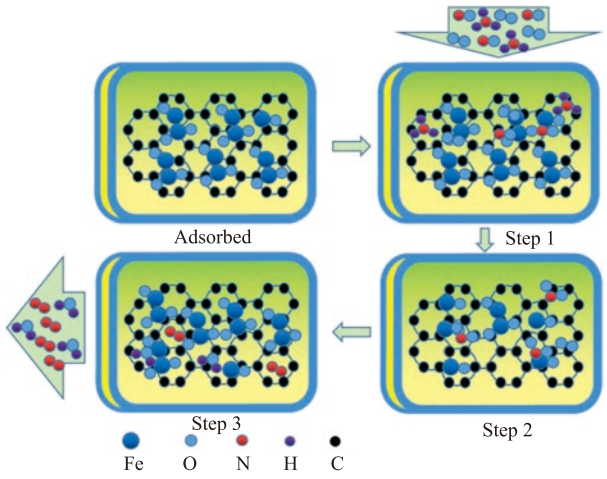

Fig.13 Denitration mechanism diagram of Fe/AC catalysts

a) The reaction gases of NH_3, NO and O_2 are continuously diffused from the catalyst's outer surface to the inner surface of Fe/AC. Numerous reactant gases can be stored, and many reaction units can be generated on the graphite microcrystalline structure inside the catalyst because of the large specific surface area and rich pore structure of AC[44]. The reaction gas is adsorbed on the surface of the catalyst in an adsorption state on the active sites of the catalyst, and the active sites then activate the reaction gas to form molecules. For example, many acidic oxygen-containing functional groups and C-H groups detected by FTIR will preferentially adsorb N; additionally, XPS can also detect that the adsorbed oxygen (O_β) content on the surface of Fe/AC catalyst is relatively high. Since surface-absorbed oxygen (O_β) has high mobility, it can promote the oxidation of NO to NO_2 and provide a highly active adsorption site for NH_3[45] (Eqs.(1)-(4)).

b) A reaction occurs between NO and NH_3. During the denitration process, an oxidation-reduction reaction between Fe^{2+} and Fe^{3+} may occur (Eqs.(5) and (6)). As demonstrated by XPS characterisation, the surface-adsorbed oxygen (O_β) is more active than lattice oxygen (O_α) because of the formation of oxygen vacancies between Fe^{2+} and Fe^{3+} in the redox reaction, which significantly promotes the continuous replenishment of (O_β). The transformation from the standard SCR reaction to the fast SCR reaction (Eqs. (7) and (8)) is accelerated. This phenomenon may be due to the increased mobility of the active substance or oxygen, which is conducive to the denitration reaction.

c) The gas (N_2 and H_2O) generated from the surface of the catalyst is desorbed and diffused to the inner surface through the AC pores, and then the gas diffuses from the inner surface of the AC to the outer surface of the Fe/AC catalyst (Eqs.(9) and (10)).

Based on the above findings, the valence of Fe ions on the surface of the Fe/AC catalyst increases, as does the amount of adsorbed oxygen (O_β) on the surface increases (O_β). The Fe/AC catalyst can absorb more reaction gases as the surface acid functional groups increase. The accumulation of all factors results in Fe/AC achieving significant NH_3-SCR denitration efficiency.

$$NH_3(g) \rightarrow NH_3(ads) \quad (1)$$

$$NO(g) \rightarrow NO(ads) \quad (2)$$

$$O_2(g) \rightarrow O_2(ads) \quad (3)$$

$$NO(ads) + O_2(ads) \rightarrow NO_2(ads) \quad (4)$$

$$Fe^{3+} + NO(ads) + O_2(ads) \rightarrow Fe^{2+} + NO_2(ads) \quad (5)$$

$$Fe^{2+} + NO_2(ads) \rightarrow Fe^{2+}(NO)_2 \rightarrow Fe^{3+} + N_2(ads) \quad (6)$$

$$NH_3(ads) + O_2(ads) + NO(ads) \rightarrow N_2(ads) + H_2O(ads) \quad (7)$$

$$NH_3(ads) + NO_2(ads) + NO(ads) \rightarrow N_2(ads) + H_2O(ads) \quad (8)$$

$$H_2O(ads) \rightarrow H_2O(g) \quad (9)$$

$$N_2(ads) \rightarrow N_2(g) \quad (10)$$

6 Conclusions

In this study, an equal volume impregnation method was used to prepare a series of Fe/AC catalysts with different loads and calcination temperatures. The effects of different loads and roasting temperatures on the efficiency of NH_3-SCR denitration were studied, and the following conclusions were drawn:

a) when the roasting temperature remains constant, iron oxide crystals formed by increasing the loading amount can enter the AC pore structure; these crystals are stacked to form more micropores, thereby improving the adsorption performance of the reaction gas.

b) When the loading amount of Fe is kept constant and the roasting temperature is increased from 400 to 500 ℃, the iron oxide is mainly converted from α-Fe_2O_3 to γ-Fe_2O_3, thereby enhancing iron oxide dispersion and providing more active sites for denitration; these changes are conducive to gas adsorption, and they cause an enhanced denitration effect.

c) Fe_2O_3, the active component of Fe/AC catalysts, is highly dispersed as spherical particles on the AC surface and has good thermal stability. Increasing the number of acidic oxygen-containing functional groups on the surface of Fe/AC catalysts, such as carboxyl group and lactone groups, will provide more active adsorption sites for the denitration reaction.

d) Based on the redox reaction between Fe^{2+} and Fe^{3+}, active oxygen vacancies are formed, which increases the amount of adsorbed oxygen (O_β) on the surface, especially the increase of surface acid sites, which promotes and adsorbs more reaction gases (NH_3, O_2, NO), resulting in the conversion of the standard SCR reaction to fast SCR reaction.

Conflict of interest

All authors declare that there are no competing interests.

References

[1] Liu Y X, Zhang J, Pan J F, *et al*. Investigation on the Removal of NO from SO_2-Containing Simulated Flue Gas by an Ultraviolet/Fenton-Like Reaction[J]. *Energy Fuels*, 2012, 26(9): 5 430-5 436

[2] Song X Y, Ma X L, Ning G Q, *et al*. Pitch-Based Nitrogen-Doped Mesoporous Carbon for Flue Gas Desulfurization[J]. *Ind. Eng. Chem. Res*., 2017, 56(16): 4 743-4 749

[3] Ye J H, Shang J, Li Q, *et al*. The Use of Vacuum Ultraviolet Irradiation to Oxidize SO_2 and NO_x for Simultaneous Desulfurization and Denitrification[J]. *J. Hazard. Mater.*, 2014, 271: 89-97

[4] Zhan S H, Zhang H, Zhang Y, *et al*. Efficient NH_3-SCR Removal of NO_x with Highly Ordered Mesoporous WO_3(chi)-CeO_2 at Low Temperatures[J]. *Appl. Catal. B-Environ*., 2017, 203: 199-209

[5] Meng D M, Zhan W C, Guo Y, *et al*. A Highly Effective Catalyst of Sm-Mn Mixed Oxide for the Selective Catalytic Reduction of NO_x with Ammonia: Effect of the Calcination Temperature[J]. *J. Mol. Catal. A-Chem.*, 2016, 420: 272-281

[6] Liu Y, Ning P, Li K, *et al*. Simultaneous Removal of NO_x and SO_2 by Low-Temperature Selective Catalytic Reduction over Modified Activated Carbon Catalysts[J]. *Russ. J. Phys. Chem. A+*, 2017, 91(3): 490-499

[7] Nieto-Delgado C, Gutierrez-Martinez J, Rangel-Mendez J R. Modified Activated Carbon with Interconnected Fibrils of Iron-Oxyhydroxides using Mn^{2+} as Morphology Regulator, for a Superior Arsenic Removal from Water[J]. *J. Environ. Sci*., 2019, 76: 403-414

[8] Jiang L J, Liu Q C, Zhao Q, *et al.* Promotional Effect of Ce on the SCR of NO with NH_3 at Low Temperature over MnO_x supported by Nitric Acid-Modified Activated Carbon[J]. *Res. Chem. Intermediater*., 2018, 44(3): 1 729-1 744

[9] Nielsen L, Biggs M J, Skinner W, *et al.* The Effects of Activated Carbon Surface Features on the Reactive Adsorption of Carbamazepine and Sulfamethoxazole[J]. *Carbon*, 2014, 80: 419-432

[10] Yang R, Huang H F, Chen Y J, *et al.* Performance of Cr-doped Vanadia/Titania Catalysts for Low-Temperature Selective Catalytic Reduction of NO_x with NH_3[J]. *Chinese J. Catal.*, 2015, 36(8): 1 256-1 262

[11] Yang J J, Qing M, Li W, *et al*. Effect of Nano $V_{(2)}O_{(5)}$, Nano $Fe_{(2)}O_{(3)}$ and Nano $V_{(2)}O_{(5)}$/Fe_2O_3 on Selective Catalytic Reduction of NO over a Modified AC Catalyst[J]. *Int. J. Oil. Gas. Coal. T*., 2016, 11(4): 387-396

[12] Xu W T, Zhou J C, Li H, *et al.* Microwave-Assisted Catalytic Reduction of NO into N_2 by Activated Carbon Supported Mn_2O_3 at Low Temperature under O_2 Excess[J]. *Fuel Process. Technol*., 2014, 127: 1-6

[13] Lei Z G, Han B, Yang K, *et al.* Influence of H_2O on the Low-Temperature NH_3-SCR of NO over V_2O_5/AC Catalyst: An Experimental and Modeling Study[J]. *Chem. Eng. J*., 2013, 215: 651-657

[14] Chen Y, Liao Y F, Chen L, *et al.* Performance of Transition Metal (Cu, Fe and Co) Modified SCR Catalysts for Simultaneous Removal of NO and Volatile Organic Compounds (VOCs) from Coal-Fired Power Plant Flue Gas[J]. *Fuel*, 2021, 289: 119 849

[15] Zhang X L, Lv S S, Zhang X C, *et al.* Improvement of the Activity and SO_2 Tolerance of Sb-modified Mn/PG Catalysts for NH_3-SCR at a Low Temperature[J]. *J. Environ. Sci*., 2021, 101: 1-15

[16] Jiang L J, Liu Q C, Ran G J, *et al.* V_2O_5-Modified Mn-Ce/AC Catalyst with High SO_2 Tolerance for Low-Temperature NH_3-SCR of NO[J]. *Chem. Eng. J*., 2019, 370: 810-821

[17] Kwon D W, Nam K B, Hong S C. The Role of Ceria on the Activity and SO_2 Resistance of Catalysts for the Selective Catalytic Reduction of NO_x by NH_3[J]. *Appl. Catal. B-Environ*., 2015, 166: 37-44

[18] Zhuang K, Zhang Y P, Huang T J, *et al.* Sulfur-Poisoning and Thermal Reduction Regeneration of Holmium-Modified Fe-Mn/TiO_2 Catalyst for Low-Temperature SCR[J]. *Journal of Fuel Chemistry and Technology*, 2017, 45(11): 1 356-1 364

[19] Liu F D, Shan W P, Lian Z H, *et al*. The Smart Surface Modification of

Fe_2O_3 by WO_x for Significantly Promoting the Selective Catalytic Reduction of NO_x with NH_3[J]. *Appl. Catal. B-Environ*., 2018, 230: 165-176

[20] Yang W W, Liu F D, Xie L J, *et al.* Effect of V_2O_5 Additive on the SO_2 Resistance of a Fe_2O_3/AC Catalyst for NH_3-SCR of NO_x at Low Temperatures[J]. *Ind. Eng. Chem. Res.*, 2016, 55(10): 2 677-2 685

[21] Yang S J, Liu C X, Chang H Z, *et al.* Improvement of the Activity of γ-Fe_2O_3 for the Selective Catalytic Reduction of NO with NH_3 at High Temperatures: NO Reduction *versus* NH_3 Oxidization[J]. *Ind. Eng. Chem. Res.*, 2013, 52(16): 5 601-5 610

[22] Xie C Y, Sun Y L, Zhu B Z, *et al.* Adsorption Mechanism of NH_3, NO, and O_2 Molecules over the Fe_xO_y/AC Catalyst Surface: a DFT-D_3 Study[J]. *New. J. Chem*., 2021, 45(6): 3 169-3 180

[23] Liang H, Zha X B, Gui K T, *et al.* A Study of Selective Catalysis Reduction Denitration Performance and Adsorption of NH_3 and NO over γ-Fe_2O_3 Catalys[J]. *Proceedings of the Csee*, 2014, 34(32): 5 734-5 740

[24] Shi X B, Chu B X, Wang F, *et al.* Mn-modified CuO, $CuFe_2O_4$ and γ-Fe_2O_3 Three-Phase Strong Synergistic Coexistence Catalyst System for NO Reduction by CO with Wider Active Window[J]. *ACS Appl. Mater. Interfaces.*, 2018, 10(47): 40 509-40 522

[25] Yao G H, Fang W, Wang X B, *et al.* Magnetic Field Effects on Selective Catalytic Reduction of NO by NH_3 over Fe_2O_3 Catalyst in a Magnetically Fluidized Bed[J]. *Energy*, 2010, 35(5): 2 295-2 300

[26] Xie S Y, Li C X, Wang G, *et al*. Enhancement of NO Catalytic Oxidation on Activated Carbon at Room Temperature by Nitric Acid Hydrothermal Treatment[J]. *Appl. Surf. Sci.*, 2019, 471: 633-644

[27] Wang D, Zhang X L, Peng J S, *et al*. Effects of Calcination Temperature on Selective Catalytic Reduction of NO_x over γ-Fe_2O_3 Catalysts Prepared with Microwave Assistance[J]. *Research of Environmental Sciences*, 2015, 28(5): 808-815

[28] Pasel J, Käßner P, Montanari B, *et al.* Transition Metal Oxides Supported on Active Carbons as Low Temperature Catalysts for the Selective Catalytic Reduction (SCR) of NO with NH_3[J]. *Appl. Catal. B-Environ*., 1998, 18(3-4): 199-213

[29] Zhan S H, Zhang H, Zhang Y, *et al.* Efficient NH_3-SCR Removal of NO_x with Highly Ordered Mesoporous $WO_3(\chi)$-CeO_2 at Low Temperatures[J]. *Appl. Catal. B-Environ*., 2017, 203:199-209

[30] Dandekar A, Baker R T K, Vannice M A. Characterization of Activated Carbon, Graphitized Carbon Fibers and Synthetic Diamond Powder using TPD and Drifts[J]. *Carbon*, 1998, 36(12): 1 821-1 831

[31] Palomo J, Ternero-Hidalgo J J, Rosas J M, *et al.* Selective Nitrogen Functionalization of Phosphorus-containing Activated Carbons[J]. *Fuel Process. Technol.*, 2017, 156: 438-445

[32] Sharma A, Dutta R K, Roychowdhury A, *et al*. Cobalt Doped CuO Nanoparticles as a Highly Efficient Heterogeneous Catalyst for Reduction of 4-Nitrophenol to 4-Aminophenol[J]. *Appl. Catal. A-Gen*., 2017, 543: 257-265

[33] Yu L, Zhou H Q, Sun J Y, *et al*. Cu Nanowires Shelled with Ni-Fe Layered Double Hydroxide Nanosheets as Bifunctional Electrocatalysts for Overall Water Splitting[J]. *Energ. Environ. Sci.*, 2017, 10(8): 1 820-1 827

[34] Liu Z, Wang Z J, Qing S J, *et al*. Improving Methane Selectivity of Photo-induced CO_2 Reduction on Carbon Dots Through Modification of Nitrogen-Containing Groups and Graphitization[J]. *Appl. Catal. B-Environ.*, 2018, 232: 86-92

[35] Yu J H, So J H. Synthesis and Characterization of Nitrogen-Containing Hydrothermal Carbon with Ordered Mesostructure[J]. *Chem. Phys. Lett*., 2019, 716: 237-246

[36] Deng L L, Lu B Q, Li J L, *et al.* Effect of Pore Structure and Oxygen-Containing Groups on Adsorption of Dibenzothiophene over Activated Carbon[J]. *Fuel*, 2017, 200: 54-61

[37] Lin Y T, Li Y R, Xu Z C, *et al.* Transformation of Functional Groups in the Reduction of NO with NH_3 over Nitrogen-Enriched Activated Carbons[J]. *Fuel*, 2018, 223: 312-323

[38] Yu Y X, Tan W, An D Q, *et al*. Insight into the SO_2 Resistance Mechanism on γ-Fe_2O_3 Catalyst in NH_3-SCR Reaction: A Collaborated Experimental and DFT Study ScienceDirect[J]. *Appl. Catal. B-Environ*., 2021, 281: 119 544

[39] Wang L Y, Cheng X X, Wang Z Q, *et al.* Investigation on Fe-Co Binary Metal Oxides supported on Activated Semi-Coke for NO Reduction by CO[J]. *Appl. Catal. B-Environ*., 2017, 201: 636-651

[40] Huang B F, Shi Z, Yang Z Y, *et al*. Mechanism of CO Selective Catalytic Reduction Denitration on Fe-Mn/AC Catalysts at Medium and Low Temperatures under Oxygen Atmosphere[J]. *Chem. Eng. J*., 2022, 446(4): 137 412

[41] Pappas D K, Boningari T, Boolchand P, *et al.* Novel Manganese Oxide Confined Interweaved Titania Nanotubes for the Low-Temperature Selective Catalytic Reduction (SCR) of NO_x by NH_3[J]. *J. Catal.*, 2016, 334: 1-13

[42] Ge T T, Zhu B Z, Sun Y L, *et al.* Investigation of Low-Temperature Selective Catalytic Reduction of NO_x with Ammonia over Cr-promoted Fe/AC Catalysts[J]. *Environ. Sci. Pollut. R*., 2019, 26(32): 33 067-33 075

[43] Chen J Y, Zhu B Z, Sun Y L, *et al*. Investigation of Low-Temperature Selective Catalytic Reduction of NO_x with Ammonia over Mn-Modified Fe_2O_3/AC Catalysts[J]. *J. Braz. Chem. Soc*., 2018, 29(1): 79-87

[44] Yang J, Ren S, Zhang T S, *et al.* Iron Doped Effects on Active Sites Formation over Activated Carbon supported Mn-Ce Oxide Catalysts for Low-Temperature SCR of NO-ScienceDirect[J]. *Chem. Eng. J*., 2020, 379: 122 398

[45] Zhu L, Zhang L, Qu H X, *et al*. A Study on Chemisorbed Oxygen and Reaction Process of Fe-CuO_x/ZSM-5 via Ultrasonic Impregnation Method for Low-Temperature NH_3-SCR[J]. *J. Mol. Catal. A-Chem*., 2015, 409: 207-215